Marine Geology 419 (2020) 106044

Contents lists available at ScienceDirect

Marine Geology

journal homepage: www.elsevier.com/locate/margo

Increasing hypoxia in the Changjiang Estuary during the last three decades deciphered from sedimentary redox-sensitive elements

Yijing Wu[a], Daidu Fan[a,b,*], Deli Wang[c], Ping Yin[d]

[a] State Key Laboratory of Marine Geology, Tongji University, Shanghai 200092, China
[b] Laboratory of Marine Geology, Qingdao National Laboratory for Marine Science and Technology, China
[c] State Key Laboratory of Marine Environmental Science, Xiamen University, China
[d] Qingdao Institute of Marine Geology, China

ARTICLE INFO

Editor: Shu Gao

Keywords:
Coastal hypoxia
Sediment core
Redox sensitive elements
Changjiang Estuary

ABSTRACT

Ranked as one of the world's largest seasonal hypoxic water bodies (Dissolved oxygen, DO ≤ 2 mg l^{-1}), the Changjiang hypoxia has been reported to grow rapidly worse in recent decades according to cruise observations, but it has been seldom studied by sedimentary records. In this paper, four gravity cores (E1-E4), retrieved from the Changjiang Estuary, were dated by excess ^{210}Pb and analyzed with grain-size compositions, total organic carbon (TOC) contents, and RSEs (redox sensitive elements) compositions. We aim to decipher RSEs enrichment characteristics and controlling mechanisms in the Changjiang Estuary. The results show that Mo and V enrichment is highly promoted by particle absorption and Fe—Mn redox cycling at the shallow estuarine environment (E1 and E2) with occasional hypoxic disturbances. Scavenging of Mo and V by organic complexation becomes significant at the hypoxic center (E3), together with great influence by Fe—Mn redox cycling, but they do not work effectively for U enrichment because of its easy remobilization and abundant riverine input. Moreover, upcore increasing trends of Mo, V, and U in E3 match well with a general lowering trend of bottom water DO minima since the mid-1980s. There are two progressive hypoxic development stages intercalated with a less DO-depleted period 1991–1997 as shown by both cruise observations and RSEs/Al records. These findings are vital to better understanding coastal hypoxic development and RSEs enrichment mechanisms in the seasonal hypoxic settings, because hypoxia is predicted to increase in the near future due to intensifying human disturbances.

1. Introduction

Recent expansion of hypoxic water (Dissolved Oxygen, DO ≤ 2 mg l^{-1}) has become a global issue, and the situation can get worse due to intensifying human activities and global warming (Diaz, 2001; Keeling et al., 2009; Bianchi et al., 2010; Rabalais et al., 2010; Melzner et al., 2013; Du et al., 2018). More and more productive coastal ecosystems have been reported to undergo severe ecological degradation because of hypoxia (Diaz and Rosenberg, 2008; Stramma et al., 2010). Off the Changjiang Estuary exists one of the world's largest hypoxic water bodies, attracting increased concerns due to its fast growing hypoxic area and continuous decrease in bottom water DO minima (Chen et al., 2007; Z.Y. Zhu et al., 2016; Lu et al., 2017). The Changjiang hypoxia was first detected by a cruise survey in the mid-1950s (Gu, 1980), but its adverse impacts on the ecosystem have only been recognized in the last two decades (Li et al., 2002; Wei et al., 2007; Zhang et al., 2016). The bottom water DO concentration in the Changjiang Estuary usually starts to decline in June and rise again in October, and its core area may develop into a hypoxic state during the period from July to September with a worst situation in August. The lowest DO value so far has never been reported to fall below 0.15 mg l^{-1}, the upper threshold of the suboxic state (Song, 2008; Zhu et al., 2011, 2017; Wang et al., 2012; Ni et al., 2016; Wei et al., 2016; Lu et al., 2017; Luo et al., 2018).

The development of Changjiang hypoxia has been hypothesized to be majorly triggered by the strengthening organic-matter decomposition and water-column stratification in summer (Chen et al., 2007; Wang, 2009; Zhu et al., 2011; Z.Y. Zhu et al., 2016; Chen et al., 2015, 2017; J. Zhu et al., 2016; Wang et al., 2017). The intrusion of low DO oceanic watermass also has a certain contribution to hypoxic development (Wang et al., 2012; Qian et al., 2017). Due to complex impacts of physical, chemical and biological processes, the bottom water DO concentration of the Changjiang hypoxia varies significantly over different time scales, ranging from semi-diurnal tidal cycle (Zhu et al.,

* Corresponding author at: School of Ocean and Earth Science, Tongji University, Shanghai 200092, China.
E-mail address: ddfan@tongji.edu.cn (D. Fan).

https://doi.org/10.1016/j.margeo.2019.106044
Received 22 May 2019; Received in revised form 14 July 2019; Accepted 8 September 2019
Available online 13 September 2019

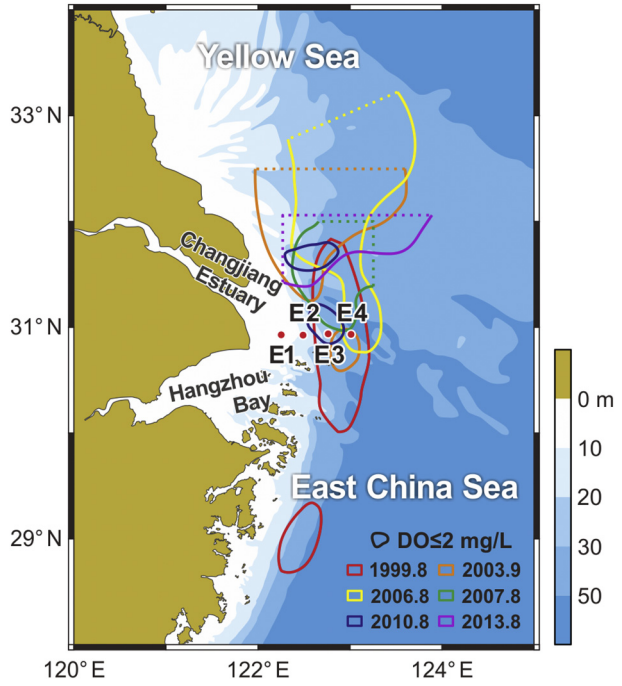

Fig. 1. Changes of hypoxic zones ($DO \leq 2\,mg\,l^{-1}$) off the Changjiang Estuary with the locations of four cores E1 to E4 (see Table S1 and references therein for original data of hypoxic areas).

2017), through to seasonal and interannual cycles (Ni et al., 2016; Wang et al., 2017), and to long-term oscillations related to climate variability (Wang et al., 2014; J. Zhao et al., 2015; Chen et al., 2017). Albeit notable annual variation in hypoxia distributions, a core area (122°30′-123°E, 30°50′-31°30′N) has been frequently mapped by cruise observations (Fig. 1; Li et al., 2002; Wang, 2009; Zhu et al., 2011 ; Wei et al., 2016).

Sediment cores are valuable to reconstruct historic hypoxia occurrences, especially where long-term instrumental DO records are not available. Moreover, proxy data can extend time spans far longer than cruise observations, crucial for better understanding the development mechanism of coastal hypoxia (Cooper and Brush, 1991; Adelson et al., 2001; Osterman et al., 2008; Zillén et al., 2008; Helz and Adelson, 2013; Erhardt et al., 2014). Mo, V and U are long considered good paleoredox proxies. They have been widely used to identify the anoxic state in silled or semi-silled basins (Brumsack, 1989; Sohlenius and Westman, 1998; Nägler et al., 2005; Noordmann et al., 2015; Hardisty et al., 2016), but less for the seasonal hypoxic state in estuaries. Xu et al. (2007) reported offshore enrichment of Mo and V at surface sediments in the Changjiang Estuary, highly contingent on the distribution of low DO water. J. Zhao et al. (2015) proposed the worsening Changjiang hypoxia after the late 1960s based on upcore Mo/Al enrichment in a gravity core. The similar conclusion was also reached by the increasing abundance of low-oxygen tolerant foraminiferal microfossils in the box-core sediments (Li et al., 2011). However, time resolutions of these two studies are very coarse. Enrichment mechanism of sedimentary RSEs/Al in the Changjiang hypoxia has never been well discussed so far as we know.

In this study, four sediment cores were retrieved along an E-W transect across the Changjiang hypoxic center. Core sediments were dated using depth profiles of excess ^{210}Pb ($^{210}Pb_{ex}$), and their RSEs and organic carbon contents, and grain-size compositions were analyzed. We aim to explore: (1) spatiotemporal variations in sedimentary RSEs in the Changjiang Estuary, (2) RSEs enrichment mechanisms in different estuarine sub-settings, and (3) hypoxic development history registered by sedimentary RSEs.

Table 1
Core locations, lengths, water depths, and mass accumulation rates (MAR) derived from $^{210}Pb_{ex}$ data.

Core no	Longitude (E)	Latitude (N)	Core length (cm)	Water depth (m)	MAR ($g\,cm^{-2}\,yr^{-1}$)
E1	122°15′11.70″	30°55′41.1″	130	10.4	–
E2	122°29′26.40″	30°55′30.0″	126	16.0	5.10
E3	122°45′48.70″	30°56′14.0″	132	23.0	5.87
E4	123°00′44.00″	30°55′56.4″	50	40.0	3.11

– No MAR was deduced for a less qualified fitting curve of $^{210}Pb_{ex}$ inventories of E1.

2. Materials and analytic methods

2.1. Core sampling and logging

Four sediment cores (E1-E4) were collected along a longitudinal transect (~30°55′N) with a gravity corer in March 2012 during a NSFC-supported spring cruise aboard the *R/V Haijian-46* (Fig. 1; Table 1). These cores were immediately stored in a frozen (−2°C) chamber after collection. The frozen cores were removed to the core laboratory and kept in normal room temperature for two days before they were split lengthwise into two halves. The archived halves were wrapped with polyethylene film and preserved under 4 °C, and the working halves were photographed, lithologically described, and nondestructively analyzed by XRF core scanner (data not shown here) before subsampling at an 1-cm interval. The sediment subsamples were sealed in numbered polyethylene bags for further analysis.

2.2. Laboratory analysis and data processes

For each core, 13–18 g sediment subsamples were selected at 4–10 cm intervals, and dried at 60 °C for 48 h to determine water contents. Activities of total ^{210}Pb ($^{210}Pb_t$), ^{137}Cs and ^{226}Ra in these subsamples were determined using a low background HPGe γ-ray detector (EG& G Ortec Ltd., USA) at the Nanjing Institute of Geography and Limnology, Chinese Academy of Sciences. The relative error of this method was reported < 10% (Guo et al., 2007). ^{226}Ra was used as an index of supported ^{210}Pb ($^{210}Pb_{su}$), and excess ^{210}Pb ($^{210}Pb_{ex}$) activities were obtained via subtracting $^{210}Pb_{su}$ activities from $^{210}Pb_t$ activities. The Constant Rate of Supply (CRS) model is generally preferred for the environments with changing sediment accumulation rates (Appleby and Oldfield, 1978). In this study, a modified CRS model was applied to reconstruct age models because gravity cores are too short to reach the horizon of $^{210}Pb_{su}$ (Sanchez-Cabeza and Ruiz-Fernández, 2012). The apparent depth (cm) was converted to cumulative mass ($g\,cm^{-2}$) on the basis of water contents, porewater density ($1.025\,g\,cm^{-3}$) and sediment dry density ($2.6\,g\,cm^{-3}$) (Huh et al., 2011; Wang et al., 2016). Fitting analysis was done using the 'Exp2PMod1' function in Origin 8.0 program.

Grain size analysis was carried out using a laser-diffraction Beckman Coulter LS230 at the State Key Laboratory of Marine Geology (SKLMG), Tongji University (Table S2). Pretreatment and parameter calculations were performed as outlined by Fan et al. (2015). Each sample was tested twice for quality control, and relative errors of repeated tests were better than 2%.

Total carbon (TC), total organic carbon (TOC), and total nitrogen (TN) were measured by an Elementar Vario Cube CN organic matter analyzer at the SKLMG (Table S3). The procedures of S.Y. Yang et al. (2011) were strictly followed to do chemical pretreatment and calibration of TOC concentrations. The analysis of duplicate samples ($n = 20$) yielded a precision of 0.2% for TC, 0.1% for TOC, and 0.02% for TN, respectively.

Metallic-oxide concentrations including Al, Fe, and Mn of bulk

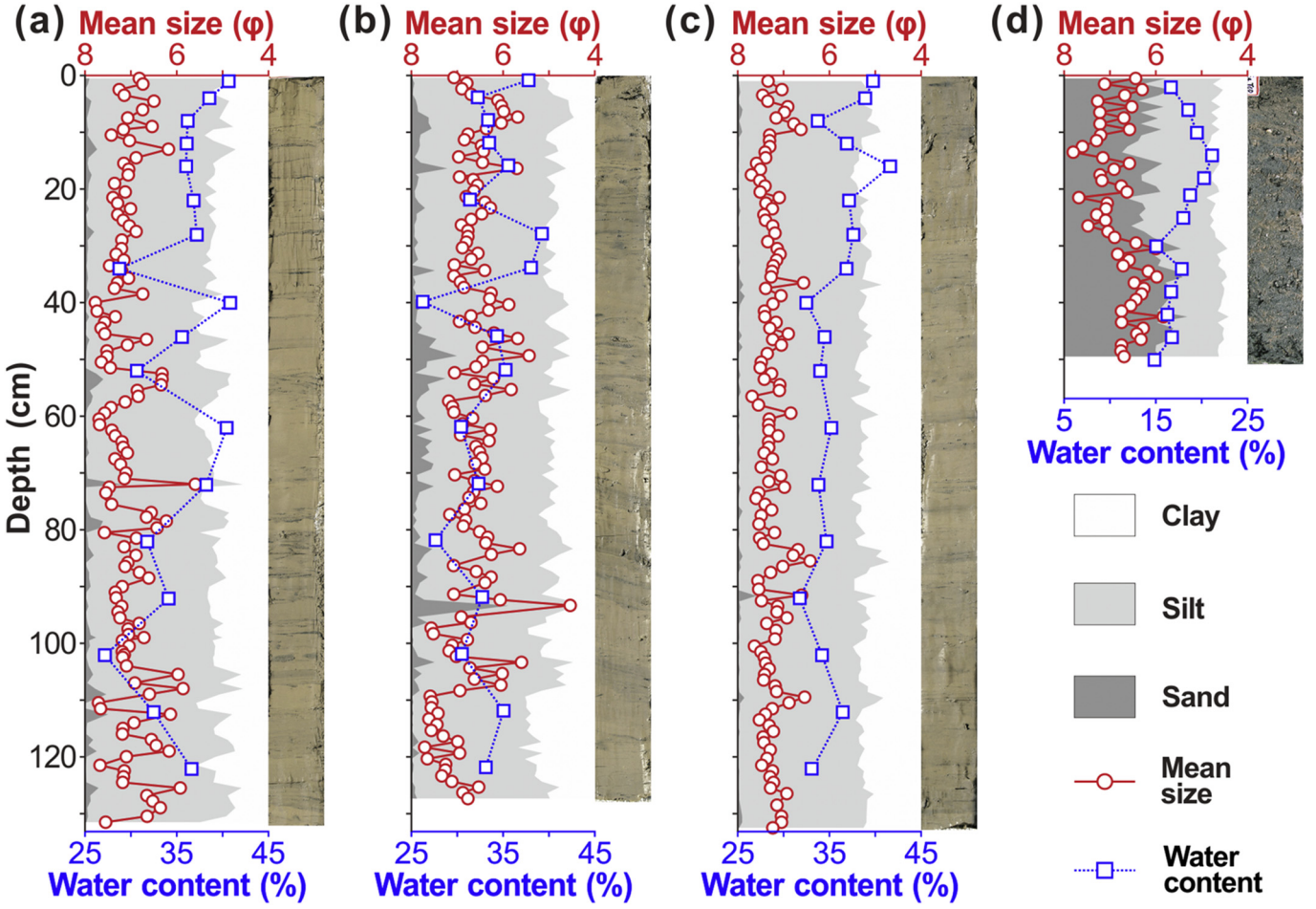

Fig. 2. Core photos, grain-size compositions, mean sizes and water contents of cores E1 (a), E2 (b), E3 (c), and E4 (d).

sediment samples were measured by an IRIS Advantage ICP-AES, and trace-elemental abundances including U, V, and Mo were measured by VG-X7 ICP-MS at the SKLMG (Table S3). We strictly followed the digestion and analytical methods established at the SKLMG and described in detail by Shao et al. (2017). Precision of measured elements were assessed using certified geochemical reference materials GSR-5, GSR-6, and GSD-9. The reproducibility of elemental concentrations in standards is close to the certified values (Table S4). The accuracy was high for all metals except for Mn in GSR-5. In nature, Mn concentrations in sediment samples are much closer to those in GSR-6 and GSD-9, and no additional adjustment was applied to Mn measurements.

3. Results

Cores E1-E3 have almost the same lithology as shown in core photos, mainly composed of pale-brownish massive mud, intercalated with numerous gray silty/sandy laminae varying from < 1 mm to 3 mm in thickness (Fig. 2). In addition, two slightly coarsening-upward sequences can be identified in E1 roughly at 80 cm below the core surface, and the upper section has a few more silty/sandy laminae than the lower section (Fig. 2a). E4 has a completely different lithology featured by dark-gray massive sand rich in shell fragments, embedded with some pale-yellowish muddy laminae or irregular patches (Fig. 2d). E4 was sampled from the paleo-river trough covered by relict sands, making it different from the other three cores in the modern delta-front and prodelta settings (Fig. 1).

The lithological similarity is also evident in the grain-size compositions of cores E1-E3, but distinctly different from those of E4 (Fig. 2). Sand is a dominant component in E4, varying from 31.69% to 67.18% with an average of 49.61%. In contrast, cores E1-E3 are predominantly composed of silt with a whole-core average of the silt component reaching 68.40% for E1, 70.56% for E2, and 67.73% for E3, respectively. In addition, the average of mean size and silty component are 8.6 μm and 70.40% for the upper 80-cm section of E1, slightly larger than the corresponding statistics (7.6 μm and 67.34%) for the lower section.

Each depth profile of $^{210}Pb_{ex}$ activities shows relatively steady exponential decay trends in cores E2-E4, which are ideal for sedimentation age reconstruction (Fig. 3). While, it is quite irregular in E1, typically with much lower $^{210}Pb_{ex}$ activities at 30–80 cm than the expected. They were not examined to link with the coarse-grain effect in that radionuclides tend to be adsorbed with fine particles. However, they can result from rapid deposition of dredged sediments because E1 was retrieved close to the former disposing location of dredged sediments by the Deep Waterway Project in the North Passage (Zhao et al., 2013). Post-storm rapid deposition of resuspended sediments could also produce lower $^{210}Pb_{ex}$ values due to mixing older deposits by erosion (Huo et al., 2011), considering that the shallow subtidal platform of the Changjiang Delta is high susceptible to storm impacts (Fan et al., 2006, 2017). Moreover, they may also link with recently increasing sediment erosion and redistribution at the shallow delta front between 5- and 10-isobath induced by sharp decrease of sediment discharge from the Changjiang River (Yang et al., 2011). Hence the irregular depth profile of $^{210}Pb_{ex}$ in E1 will not be used to reconstruct core depositional ages. Below the surface mixed layers (SMLs), fitting results give mean MARs of 5.10 g cm^{-2} yr^{-1} for E2, 5.86 g cm^{-2} yr^{-1} for E3, and 3.11 g cm^{-2} yr^{-1} for E4, respectively. Coefficient-of-determination (R^2) of the exponential fitting line shows certain fluctuations in three cores,

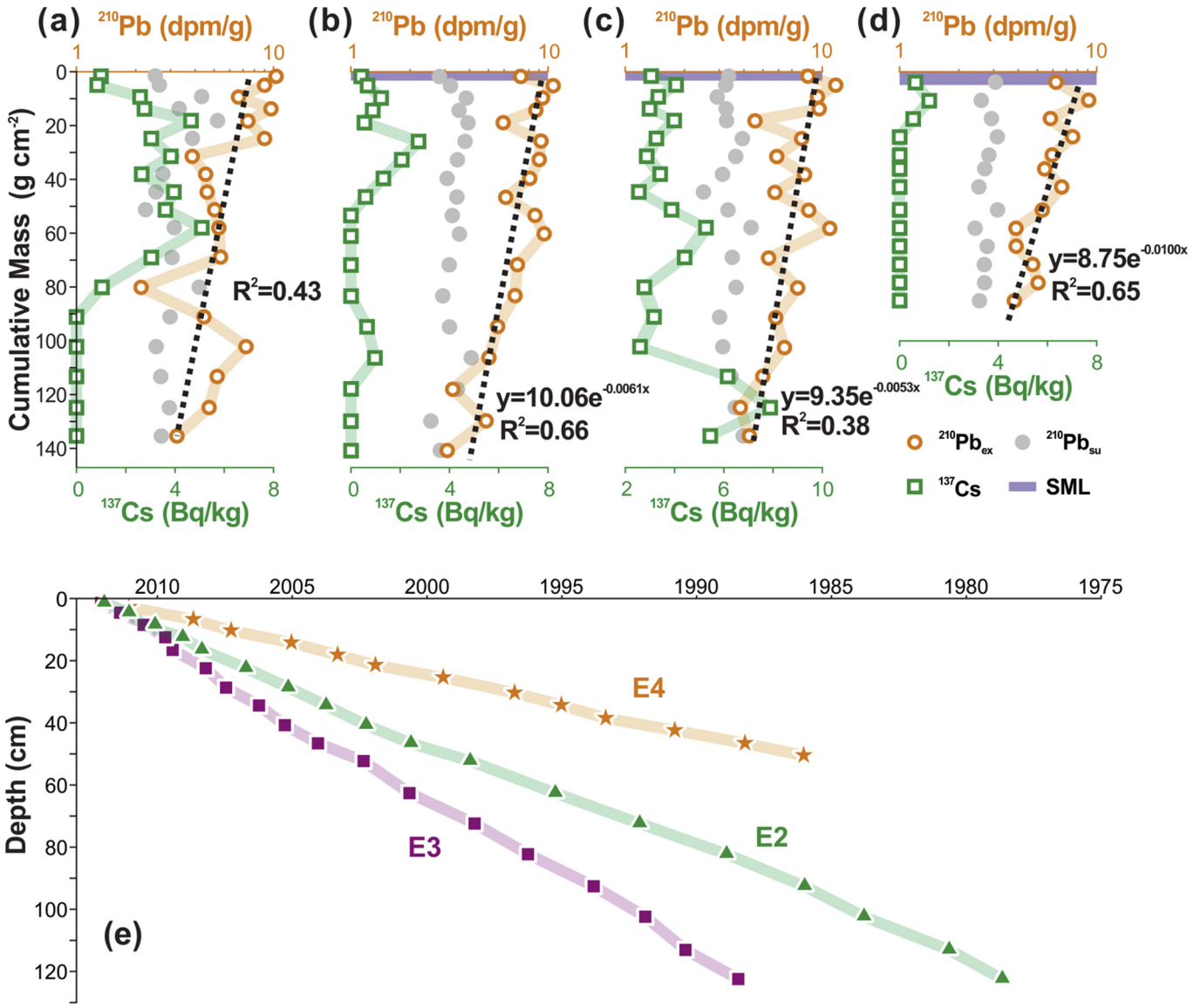

Fig. 3. Radionuclides profiles of cores E1 (a), E2 (b), E3 (c), and E4 (d), and (e) reconstructed ages by CRS (Constant Rate of Supply) model for cores E2, E3, and E4. SMLs: surface mixed layers.

therefore a modified CRS model was applied to reconstruct age models (Sanchez-Cabeza and Ruiz-Fernández, 2012). Cores E2, E3 and E4 can be dated back to the late 1970s (Fig. 3e).

Depth profiles of ^{137}Cs are usually measured at the same time to constrain $^{210}Pb_{ex}$ derived sedimentation rates and age models (Huh and Su, 1999; Huh et al., 2011). ^{137}Cs is an artificial radionuclide produced by nuclear tests, and its first appearance in the ECS deposits has been allocated to the early 1950s together with an obvious peak in 1963 (Su and Huh, 2002; Huh et al., 2011). Unfortunately, ^{137}Cs activities are too low to be detected in most depositions of E4, potentially linked with its sand-dominated lithology (Fig. 3d). Extreme low ^{137}Cs activities were also found in E2 (Fig. 3b). For E3, the first presence of ^{137}Cs is deeper than the core length (Fig. 3c), so it is difficult to assign an obvious peak at 113 cm to a certain known age (Zhang et al., 2008). Only E1 demonstrates a meaningful ^{137}Cs distribution for age reconstruction, and the first appearance depth of ^{137}Cs coincides with the above-mentioned lithological boundary (Figs. 2, 3a). However, this attempt was also given up because of strong disturbances by storms and human activities as discussed previously.

The average of TOC contents is 0.69 ± 0.17% for E2, 0.60 ± 0.11% for E3, and 0.48 ± 0.10% for E4, respectively (Fig. 4). In cores E2 and E3, TOC% shows a sharply increased step during the late-1990s (cyan bands in Fig. 4), changing from 0.66 ± 0.15% to 0.74 ± 0.19% in E2, and from 0.50 ± 0.05% to 0.67 ± 0.09% in E3. No obvious downcore variation in TOC% was observed in E4.

RSEs/Al ratios vary in relatively small ranges, with their maximum values seldom exceeding twofold their mean values in muddy deposits in the East China Sea (ECS-M, Zhao and Yan, 1994) and in the upper continental crust (UCC, Rudnick and Gao, 2003). The V/Al ratio varies between 11.3 × 10^{-4} and 16.1 × 10^{-4} for all core samples, very close to its ECS-M ratio of 13 × 10^{-4} and the UCC ratio of 12 × 10^{-4}, respectively (Fig. 4; Table 2). The U/Al ratio in all four cores changes between 0.237 × 10^{-4} and 0.561 × 10^{-4}, and its mean value for each core is only a little higher than the UCC and ECS-M values (0.28–0.33 × 10^{-4}). Mean Mo/Al ratio for each core is smaller than the UCC value (0.13 × 10^{-4}), but slightly higher than the ESC-M value (0.09 × 10^{-4}), except for E4. The relative lower mean Mo/Al value (0.065 × 10^{-4}) in E4 may stem from its predominance of sands and coarse silts, having much less effective mineral surface area for Mo absorption. In addition, two Mo/Al peaks are obvious in cores E1 and E2, but they are greatly suppressed in E3 and not observed in E4 (Fig. 4).

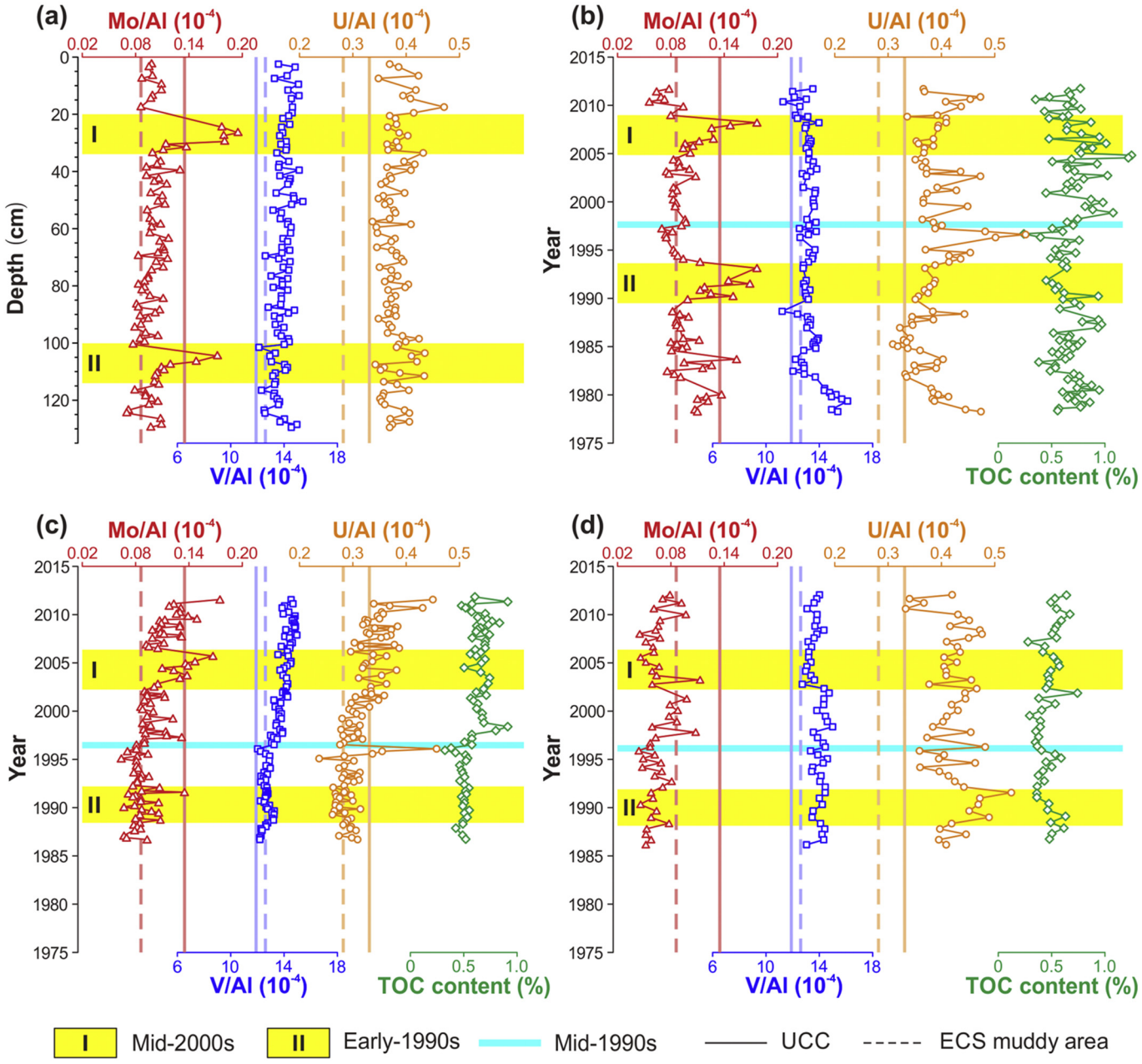

Fig. 4. Down-core variations of RSEs/Al and TOC% in cores E1 (a), E2 (b), E3 (c), and E4 (d).

Table 2
Average RSE/Al ratios and peak Mo/Al ratios in cores E1-E4.

RSE/Al	Whole/sections	E1	E2	E3	E4	ECS-M[a]	UCC[b]
V/Al (10^{-4})	Average	13.9 ± 0.6	13.3 ± 0.8	13.5 ± 0.8	13.9 ± 0.5	13	12
U/Al (10^{-4})	Average	0.38 ± 0.02	0.39 ± 0.04	0.32 ± 0.04	0.42 ± 0.04	0.28	0.33
Mo/Al (10^{-4})	Average	0.104 ± 0.023	0.098 ± 0.025	0.100 ± 0.023	0.065 ± 0.016	0.09	0.13
Mo/Al (10^{-4})	Mid-2000s	0.195*	0.176	0.174	–		
	Early-1990s	0.172*	0.176	–	–		

– No obvious peak.
* Presence of Mo/Al peaks around 30 cm and 100 cm deep in core E1.
[a] Average metal abundance in muddy deposits in the East China Sea (ECS-M, Zhao and Yan, 1994).
[b] Average metal abundance in the upper continental crust (UCC, Rudnick and Gao, 2003).

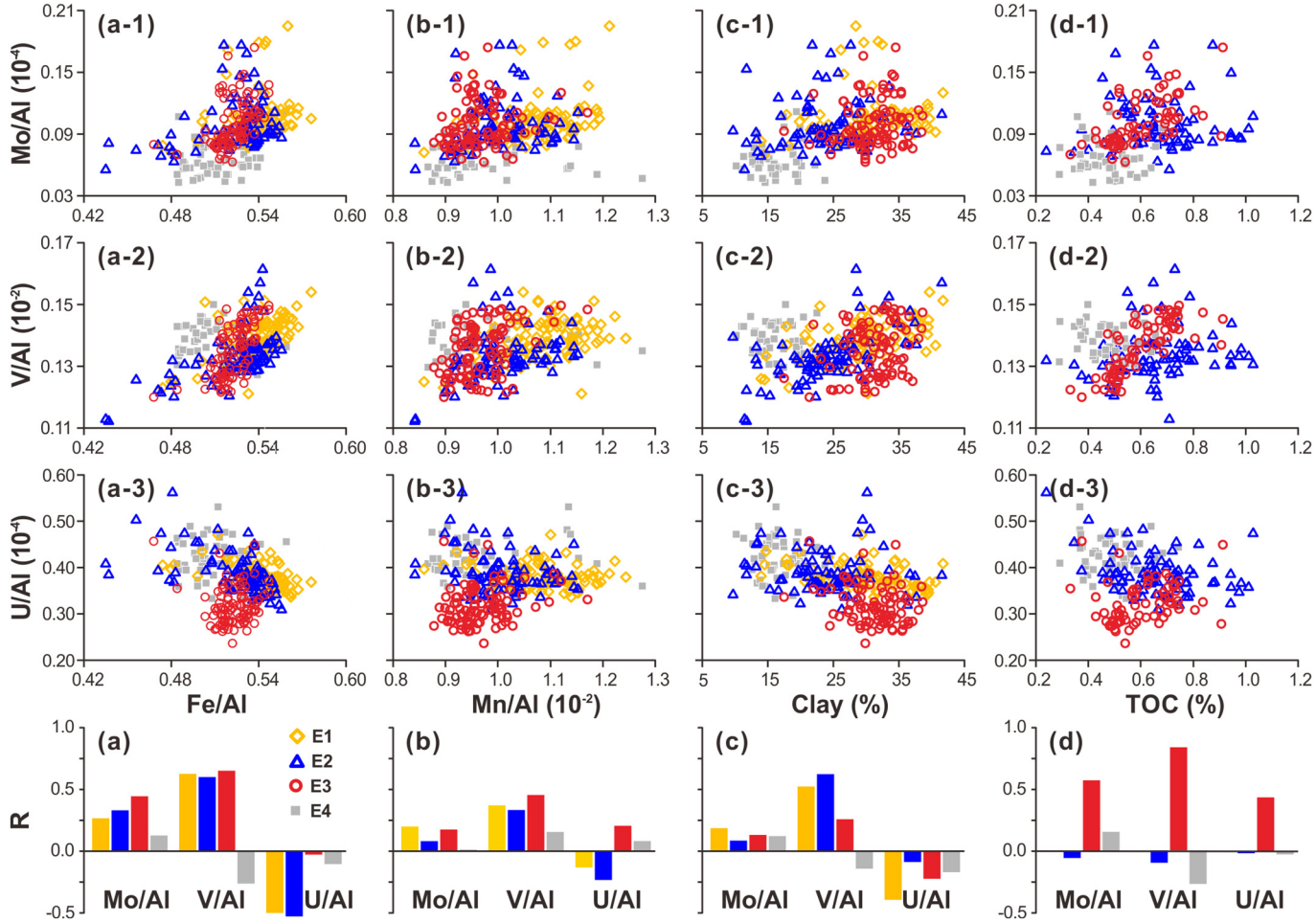

Fig. 5. Scatter plots of RSEs/Al and possible impact factors including Fe/Al (a), Mn/Al (b), clay (c), and TOC (d). Correlation coefficients (R) between different parameters are plotted at the bottom.

4. Discussion

4.1. Controlling factors of RSEs enrichment

In marine environments, multiple processes can operate simultaneously to produce RSEs enrichment (Nameroff et al., 2002; Algeo and Maynard, 2004; McManus et al., 2005; Scott and Lyons, 2012; Little et al., 2015). The change in redox states often acts as a geochemical switch to transform RSEs from conservative to particle-reactive natures, consequently altering RSEs scavenging rates in the water column and their concentrations in sediments (Tribovillard et al., 2006). In general, the enrichment of RSEs increases gradually from normoxic to anoxic environments (Sundby et al., 2004; Scott and Lyons, 2012; Helz and Adelson, 2013). Scatter plots of RSE/Al versus controlling factors are useful to assess their contributions to the formation of authigenic components (Van der Weijden, 2002). We adopted this methodology to assess the impacts of Fe–Mn redox cycling, fine particle absorption, and organic complexation on RSEs/Al enrichments in the Changjiang Estuary (Fig. 5).

In normoxic waters, Mo and V are tightly coupled with the reflux of Fe and Mn (Bertine and Turekian, 1973; Takematsu et al., 1985; Auger et al., 1999; Helz and Adelson, 2013; Bauer et al., 2017). Through Fe–Mn redox cycling, RSEs in the water column are first adsorbed onto Fe–Mn oxyhydroxides before exporting to surface sediments, but they can be released by reductive dissolution of oxyhydroxides near the water-sediment interface, dependent on the position of the chemocline (Crusius et al., 1996; Morford et al., 2005; Tribovillard et al., 2006; Algeo and Tribovillard, 2009). The mechanism of Fe and Mn refluxing should be highlighted by their roles in cycling RSEs at the water-sediment interface in response to seasonal hypoxia alternations. Authigenic Fe and Mn fractions are very high in the ECS muddy deposits, accounting for 25.1% and 73.8% of their total, respectively (Zhao and Yan, 1994). High positive correlation coefficients (R) between V/Al (Mo/Al) and Fe/Al (Mn/Al) in cores E1-E3 demonstrated an important role of Fe–Mn redox cycling in RSEs enrichments (Fig. 5a, b). In addition, the correlations between V/Al (Mo/Al) and Fe/Al have slightly higher R values than those between V/Al (Mo/Al) and Mn/Al, denoting a weaker combination of V (Mo) with Mn and Fe in the sediments. In the Changjiang Estuary, the presence of peak concentrations of interstitial Mn^{2+} was found much shallower than that of interstitial Fe^{2+} in sediment cores, indicating that early diagenesis prefers consuming Mn oxides in response to organic matter degradation (Zou et al., 2010; Zhao et al., 2017). This diagenetic preference should account for the lower correlations of RSEs/Al with Mn/Al than Fe/Al (Fig. 5a, b).

Clay contents correlate closely with V/Al ($R > 0.5$) in cores E1 and E2, but the correlation turns to weaken offshore toward E3 ($R = 0.26$). It finally changes into a negative correlation in E4 (Fig. 5c), where core sediments are predominantly composed of sands and coarse silts, without much fine-grained components (Fig. 2). A similar offshore trend of decreasing correlations between V/Al and fine-grained (< 2–$16\ \mu m$) components was reported for surface sediments in the Changjiang Estuary (Zhang et al., 2005). The offshore decrease in the contribution of fine-grained surface adsorption may also result from the competition with organic complexation as discussed below.

The correlation between TOC% and V/Al are tight in E3 ($R = 0.83$), but much poorer in E2 and E4 (Fig. 5d). In the reduced state, authigenic RSEs accumulation is primarily sensitive to the delivery and burial of organic matters (Morford and Emerson, 1999; Zheng et al., 2002; McManus et al., 2005; Algeo and Tribovillard, 2009; Wang and Sañudo Wilhelmy, 2009). On one hand, degradation of sinking organic matters directly consumes DO to trigger hypoxia in the bottom water, favoring transformation of RSEs to particle-reactive species (Gray et al., 2002; Howarth et al., 2011; Wang et al., 2016). On the other hand, organic matters could shuttle RSEs to the seafloor through sinking organometallic complexes, which are very common in the areas with high primary productivity (Morford and Emerson, 1999; Erickson and Helz, 2000; Tribovillard et al., 2006; Lyons et al., 2009). These should account for better correlations between RSEs/Al and TOC% in E3 than other cores. We also noticed that V/Al is more closely associated with TOC% than Mo/Al and U/Al in E3. Similar strong association between V and TOC was also observed in the seasonal hypoxia off the Mississippi Delta (Swarzenski et al., 2008). It was deduced that organic complexation can significantly enhance sedimentary V enrichment under the moderately reducing state like the Changjiang Estuary (Emerson and Huested, 1991; Morford and Emerson, 1999; Algeo and Maynard, 2004), but it may not have important role in sedimentary U and Mo enrichment until reaching anoxic states (Algeo and Maynard, 2004; McManus et al., 2005, McManus et al., 2006; Algeo and Lyons, 2006). The difference in the correlations between TOC% and RSEs/Al is therefore a potential new proxy to distinguish hypoxic and anoxic environments.

It is noteworthy that U/Al tends to have negative or weak ($R < 0.2$) correlations with controlling factors, except for a moderate correlation ($R = 0.27$) with TOC% in E3 (Fig. 5). This is considered to accord with the predominance of detrital U input in the Changjiang Estuary (Xu et al., 2007). Furthermore, the primary removal mechanism for U is via diffusion across the sediment-water interface under reducing conditions, and adsorption or precipitation as U-oxides within the sediments (Anderson et al., 1989; Klinkhammer and Palmer, 1991; McManus et al., 2005). Therefore, authigenic U enrichment is considered to be unrelated with redox cycling of Fe and Mn in the water column, but may participate in the formation of organometallic ligands in a reducing state (Algeo and Maynard, 2004; McManus et al., 2005; Tribovillard et al., 2006). In addition, authigenic U can be easily remobilized in response to seasonal alternations from hypoxic to normoxic settings, erasing the registered hypoxic signal accordingly (Thomson et al., 1998; Zheng et al., 2002; McManus et al., 2005). In short, U is considered less useful than Mo and V as a sedimentary indicator in the seasonal Changjiang hypoxia.

4.2. Sedimentary RSEs/Al records of hypoxic exacerbation since the mid-1980s

Four cores (E1-E4) exhibit different RSEs/Al enrichment trends in comparison with their ECS-M and UUC values (Fig. 4; Table 2; Zhao and Yan, 1994; Rudnick and Gao, 2003). Upcore variations in RSEs/Al are small in cores E1 and E4, except for two positive Mo/Al excursions identified at depths of 30 cm and 105 cm in E1. Similar Mo/Al spikes were also identified in E2, which were dated to the early 1990s and late 2000s, respectively (Fig. 6a). The U/Al curve in E2 shows significant fluctuation with a general increasing trend since the late 1980s, counter to the slight decreasing trends of Mo/Al and V/Al. The Mo/Al spikes are also seen in E3, but with a smaller magnitude. The most striking feature in E3 is the covariation of Mo/Al, V/Al, and U/Al, and their harmonious increase after the mid-1980s (Fig. S1; Fig. 4c). Maximum Mo/Al values of 0.2×10^{-4} in three cores (E1-E3) are comparable with 0.3×10^{-4} in the Chesapeake Bay (Adelson et al., 2001), but obviously $< 8.2 \times 10^{-4}$ in the Black Sea sapropels (Brumsack, 1989) and 40×10^{-4} in the Baltic Sea (Vallius and Kunzendorf, 2001). The difference may link to weaker RSEs enrichment in the seasonal coastal hypoxia than persistent deep-water hypoxia. But it may also result from significant dilution by huge terrestrial inputs, considering that sedimentation rates are orders of magnitudes higher than the Black Sea ($\sim 0.01\ cm\ yr^{-1}$, Ross, 1970;Bahr et al., 2005), and Baltic Sea ($\sim 0.5\ cm\ yr^{-1}$, Kunzendorf et al., 2001).

To explore the potential linkage of RSEs/Al enrichment with hypoxic events, time-series observational data were collected from recent publications or annual official reports (Fig. 6). The post-1985 period was chosen because both core proxy records and systematic observations of hypoxia are available. Because the Changjiang hypoxia usually occurs between July and September with the minimum DO occurrence in August (Song, 2008; Zhu et al., 2011, 2017), hypoxic data from August surveys were selected. However, other monthly survey data were used for the years 2003 and 2010, because no hypoxic record is available for August in 2010, and benthic DO depletion was peaked in September for 2003 (Wei et al., 2007; Chen et al., 2007).

The compiled DO observation data show that there were two severe hypoxic periods in the early 1990s and mid-2000s, respectively, and minimum DO concentrations declined continuously in the recent decade (Fig. 6c). Development of coastal hypoxia has often been linked to increasing riverine nutrient inputs, coeval with HAB (harmful algae bloom) increases in the Changjiang Estuary and adjacent waters (Zhang et al., 2016). Degradation of sinking organic matter after algal blooms has also been widely cited as hypoxia triggers (Zhou et al., 2008; Howarth et al., 2011; Wang et al., 2016). This is well corroborated by historical records of two HAB outbreaks in the early 1990s and mid-2000s (Fig. 6d), coincident with the two extreme hypoxic periods.

The comparison shows that two hypoxic development stages with a boundary in the late 1990s were well registered by sedimentary RSEs/Al and TOC signals in E3, retrieved from the hypoxic center (Fig. 6b). The upper section deposited over the recent decade has stronger RSEs/Al enrichment, corresponding to more frequent and severe hypoxic events, and its elevated TOC contents coincides with contemporary increasing HAB outbreaks, which in turn are highly contingent on recently elevated nutrient concentrations (Fig. 6e, f). In the lower section, more stable and lower TOC contents mirrored the less frequent HAB occurrences during the mid-1980s to late-1990s (Fig. 6c). However, DO observation data are sparse in this earlier stage, with only three records available from the late 1980s. The documental absence of hypoxia events between 1991 and 1997 were simply assumed no significant hypoxic occurrences, which are coeval with few HABs (Fig. 6c, d), although the outbreak of HABs is not a prerequisite to hypoxic occurrences in the Changjiang Estuary (Wei et al., 2007; Wang, 2009; Zhu et al., 2011, 2017; Luo et al., 2018). Weaker RSEs/Al enrichment in E3 also supports the assumption of fewer hypoxic events at that time (Fig. 6b).

Except for two positive Mo/Al excursions, no obvious RSEs/Al enrichments were observed in cores E1 and E2. We attribute this to their marginal positions in relation to the hypoxic center, and shallower water depths (Fig. 1). This is consistent with previous studies that Mo and V concentrations in nearshore surface sediments were mainly controlled by terrestrial inputs, and significant enrichments of these elements occurred only in the recent hypoxic center (Xu et al., 2007). Moreover, it is interesting to find that two Mo/Al spikes in E2 were nearly coincident with increasing in hypoxia and HABs in the early 1990s and mid-2000s (Fig. 6). The small time difference between them may result from the assumption of constant surface age for $^{210}Pb_{ex}$ chronology. Some severe hypoxic events with expanding area could reach these two core sites. The hypoxia in 2006 was reported to cover an area of 15,400 to 19,600 km^2 (Zhou et al., 2010; Zhu et al., 2011), potentially stretching onshore to the E2 location. While, the complex Mo enrichment mechanism in the shallow water should be examined carefully by taking resuspension, reoxidation and other processes into consideration.

Bulk sediment analysis of E4 shows a slight Mo/Al deficiency, minor V/Al enrichment, and moderate U/Al enrichment (Fig. 4; Table 2). The

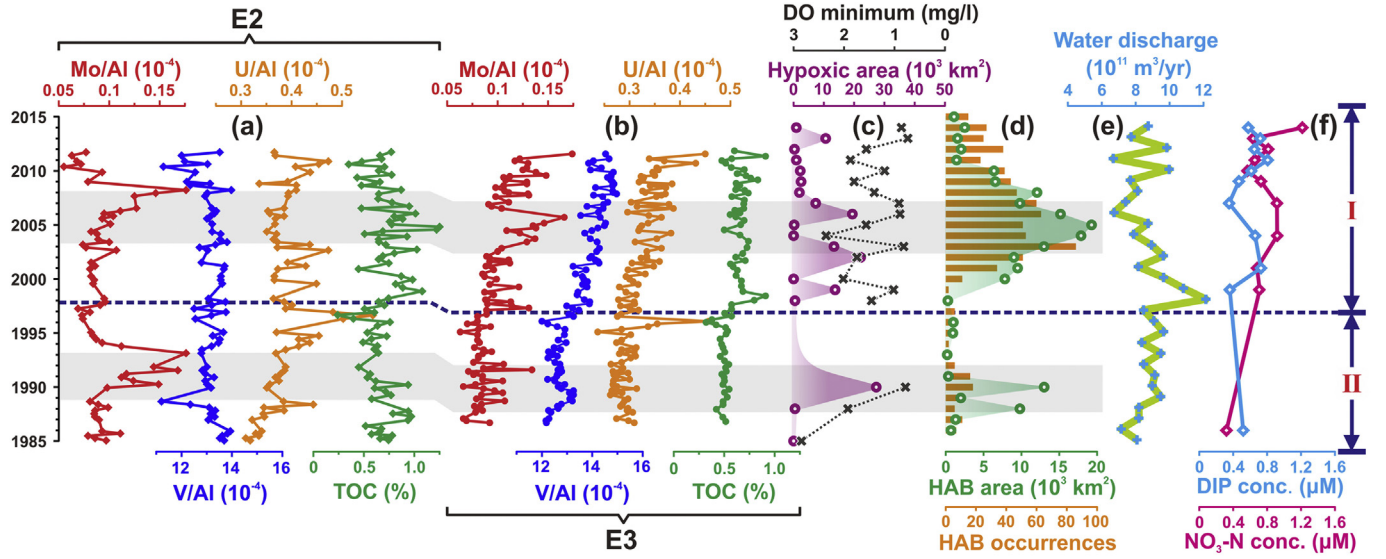

Fig. 6. Comparisons of hypoxic occurrences between cruise observations and sedimentary records. Sedimentary RSEs/Al values in cores E2 (a) and E3 (b), (c) observation data of minimum DO concentrations and hypoxic areas (Table S4), (d) annual official reports of HAB occurrences and affected areas (Tang, 2009; SOA, 2015), (e) annual water discharge at the Datong station (Y.F. Zhao et al., 2015), and (f) DIP and NO_3-N concentrations in the Changjiang Estuary (Liang and Xian, 2018). The shaded areas mark two severe hypoxic periods in the early 1990s and mid-2000s, respectively, with their boundary indicated by the dark blue dashed line. (For interpretation of the references to colour in this figure legend, the reader is referred to the web version of this article.)

core was retrieved from the paleo-river trough with a water depth of 40–60 m. Such a depressed topography intruded by the low DO shelf watermass should favor hypoxia development (Wei et al., 2007; Qian et al., 2017). However, the location of E4 is covered by relict sands, with an average sand percentage of 49.6% (Fig. 2). The sand-dominant lithology in E4 bears distinctly different RSEs/Al compositions from the nearby core E3 dominated by mud. The Yangtze Shoal, north of the paleo-river trough, which is also covered by relict sands, has become increasingly influenced by the recently northward expanding hypoxia (Fig. 2; Wei et al., 2007; Zhu et al., 2011, 2017; Lu et al., 2017). The less known RSEs behaviors in the relict sands in response to enhancing hypoxia (Tyson and Pearson, 1991) deserves further investigation.

5. Conclusions

(1) Enrichment of Mo, V, and U is moderate in the Changjiang Estuary, seldom exceeding twice their regional mean concentrations in the East China Sea, and TOC contents are also relatively low with individual core averages ranging from 0.48 to 0.69%, denoting obvious dilute effects by high accumulation rates between 3.11 and 5.87 $g\,cm^{-2}\,yr^{-1}$.

(2) The impact of Fe−Mn redox cycling is obvious on Mo and V enrichment, but not for U enrichment because of its easy remobilization and marked riverine input in the Changjiang Estuary. The role of particle absorption in Mo and V enrichment declines offshore. In the offshore hypoxic region, organic complexation becomes important in RSEs enrichment. In comparison, Mo and V are more sensitive than U to seasonal occurrences of coastal hypoxia.

(3) Two progressive hypoxic development stages were clearly identified from sedimentary RSEs at E3 in the Changjiang hypoxic center, coincident very well with two periods having more severe hypoxia and HAB occurrences based on cruise observation data. A few severe hypoxic events with expanding area were also registered in the nearshore core E2. In short, RSEs can be used as a good proxy to study hypoxia which occurs only seasonally with moderate depletion of bottom water dissolved oxygen (DO) such as the Changjiang hypoxia.

Supplementary data to this article can be found online at https://doi.org/10.1016/j.margeo.2019.106044.

Acknowledgments

This research was funded by the National Natural Science Foundation of China (NSFC-41776052, 41730531), Qingdao National Laboratory for Marine Science and Technology (MGQNLM-TD201802), and the Research Fund of State Key Laboratory of Marine Geology at Tongji University (Grant no. MG20190104).

References

Adelson, J.M., Helz, G.R., Miller, C.V., 2001. Reconstructing the rise of recent coastal anoxia; molybdenum in Chesapeake Bay sediments. Geochim. Cosmochim. Acta 65 (2), 237–252.
Algeo, T.J., Lyons, T.W., 2006. Mo-total organic carbon covariation in modern anoxic marine environments: Implications for analysis of paleoredox and paleohydrographic conditions. Paleoceanography 21 (1), PA1016.
Algeo, T.J., Maynard, J.B., 2004. Trace-element behavior and redox facies in core shales of Upper Pennsylvanian Kansas-type cyclothems. Chem. Geol. 206 (3–4), 289–318.
Algeo, T.J., Tribovillard, N., 2009. Environmental analysis of paleoceanographic systems based on molybdenum–uranium covariation. Chem. Geol. 268 (3–4), 211–225.
Anderson, R.F., Lehuray, A.P., Fleisher, M.Q., Murray, J.W., 1989. Uranium deposition in Saanich Inlet sediments, Vancouver Island. Geochim. Cosmochim. Acta 53 (9), 2205–2213.
Appleby, P.G., Oldfield, F., 1978. The calculation of lead-210 dates assuming a constant rate of supply of unsupported ^{210}Pb to the sediment. Catena 5 (1), 1–8.
Auger, Y., Bodineau, L., Leclercq, S., Wartel, M., 1999. Some aspects of vanadium and chromium chemistry in the English channel. Cont. Shelf Res. 19 (15–16), 2003–2018.
Bauer, S., Blomqvist, S., Ingri, J., 2017. Distribution of dissolved and suspended particulate molybdenum, vanadium, and tungsten in the Baltic Sea. Mar. Chem. 196, 135–147.
Bertine, K.K., Turekian, K.K., 1973. Molybdenum in marine deposits. Geochim. Cosmochim. Acta 37 (6), 1415–1434.
Bianchi, T.S., DiMarco, S.F., Cowan Jr., J.H., Hetland, R.D., Chapman, P., Day, J.W., Allison, M.A., 2010. The science of hypoxia in the Northern Gulf of Mexico: a review. Sci. Total Environ. 408 (7), 1471–1484.
Brumsack, H.J., 1989. Geochemistry of recent TOC-rich sediments from the Gulf of California and the Black Sea. Geol. Rundsch. 78 (3), 851–882.
Bahr, A., Lamy, F., Arz, H., Kuhlmann, H., Wefer, G., 2005. Late glacial to Holocene climate and sedimentation history in the NW Black Sea. Mar. Geol 214, 309–322.
Chen, C.C., Gong, G.C., Shiah, F.K., 2007. Hypoxia in the East China Sea: one of the largest coastal low-oxygen areas in the world. Mar. Environ. Res. 64 (4), 399–408.
Chen, X.F., Shen, Z.Y., Li, Y.Y., Yang, Y., 2015. Physical controls of hypoxia in waters adjacent to the Yangtze Estuary: a numerical modeling study. Mar. Pollut. Bull. 97 (1–2), 349–364.
Chen, J.Y., Pan, D.L., Liu, M.L., Mao, Z.H., Zhu, Q.K., Chen, N.H., Zhang, X.Y., Tao, B.Y., 2017. Relationships between long-term trend of satellite-derived Chlorophyll-a and

hypoxia off the Changjiang Estuary. Estuar. Coasts 40 (4), 1–11.
Cooper, S.R., Brush, G.S., 1991. Long-term history of Chesapeake bay anoxia. Science 254 (5034), 992–996.
Crusius, J., Calvert, S., Pedersen, T., Sage, D., 1996. Rhenium and molybdenum enrichments in sediments as indicators of oxic, suboxic and sulfidic conditions of deposition. Earth Planet. Sci. Lett 145 (1-4), 65–78.
Diaz, R.J., 2001. Overview of hypoxia around the world. J. Environ. Qual. 30 (2), 275–281.
Diaz, R.J., Rosenberg, R., 2008. Spreading dead zones and consequences for marine ecosystems. Science 321 (5891), 926–929.
Du, J., Shen, J., Park, K., Wang, Y.P., Yu, X., 2018. Worsened physical condition due to climate change contributes to the increasing hypoxia in Chesapeake Bay. Sci. Total Environ. 630, 707–717.
Emerson, S.R., Huested, S.S., 1991. Ocean anoxia and the concentrations of molybdenum and vanadium in seawater. Mar. Chem. 34 (3–4), 177–196.
Erhardt, A.M., Reimers, C.E., Kadko, D., Paytan, A., 2014. Records of trace metals in sediments from the Oregon shelf and slope: investigating the occurrence of hypoxia over the past several thousand years. Chem. Geol. 382, 32–43.
Erickson, B.E., Helz, G.R., 2000. Molybdenum (VI) speciation in sulfidic waters: Stability and lability of thiomolybdates. Geochim. Cosmochim. Acta 64 (7), 1149–1158.
Fan, D., Guo, Y., Wang, P., Shi, Z., 2006. Crossshore variations in morphodynamic processes of an open-coast mudflat in the Changjiang Delta: with an emphasis on storm impacts. Cont. Shelf Res. 26, 517–538.
Fan, D., Shang, S., Cai, G., Tu, J., 2015. Distinction and grain-size characteristics of intertidal heterolithic deposits in the middle Qiantang Estuary (East China Sea). Geo-Mar. Lett. 35 (3), 161–174.
Fan, D., Wu, Y., Zhang, Y., Burr, G., Huo, M., Li, J., 2017. South Flank of the Yangtze Delta: past, present and future. Mar. Geol. 392, 78–93.
Gray, J.S., Wu, R.S., Or, Y.Y., 2002. Effects of hypoxia and organic enrichment on the coastal marine environment. Mar. Ecol. Prog. Ser. 238, 249–279.
Gu, H.K., 1980. The maximum value of dissolved oxygen in its vertical distribution in yellow sea. Acta Oceanol. Sin. 2 (2), 70–80 (in Chinese with English abstract).
Guo, Z., Lin, T., Zhang, G., Zheng, M., Zhang, Z., Hao, Y., Fang, M., 2007. The sedimentary fluxes of polycyclic aromatic hydrocarbons in the Yangtze River Estuary coastal sea for the past century. Sci. Total Environ. 386 (1–3), 33–41.
Hardisty, D.S., Riedinger, N., Planavsky, N.J., Asael, D., Andren, T., Jorgensen, B.B., Lyons, T.W., 2016. A Holocene history of dynamic water column redox conditions in the Landsort Deep, Baltic Sea. Am. J. Sci. 316 (8), 713–745.
Helz, G.R., Adelson, J.M., 2013. Trace element profiles in sediments as proxies of dead zone history; rhenium compared to molybdenum. Environ. Sci. Technol. 47 (3), 1257–1264.
Howarth, R., Chan, F., Conley, D.J., Garnier, J., Doney, S.C., Marino, R., Billen, G., 2011. Coupled biogeochemical cycles: eutrophication and hypoxia in temperate estuaries and coastal marine ecosystems. Front. Ecol. Environ. 9 (1), 18–26.
Huh, C.-A., Su, C.-C., 1999. Sedimentation dynamics in the East China Sea elucidated from ^{210}Pb, ^{137}Cs and ^{239,240}Pu. Mar. Geol. 160, 183–196.
Huh, C.A., Chen, W., Hsu, F.H., Su, C.C., Chiu, J.K., Lin, S., Liu, C.S., Huang, B.J., 2011. Modern (< 100 years) sedimentation in the Taiwan Strait: rates and source-to-sink pathways elucidated from radionuclides and particle size distribution. Cont. Shelf Res. 31 (1), 47–63.
Huo, M., Fan, D., Xu, G., 2011. Sedimentation rates of Nanhui tidal flats in the Changjiang Delta and analysis of their influence factors. J. Palaeogeogr. 13 (1), 111–118 (in Chinese with English abstract).
Keeling, R.F., Körtzinger, A., Gruber, N., 2009. Ocean deoxygenation in a warming world. Annu. Rev. Mar. Sci. 2, 199–229.
Klinkhammer, G.P., Palmer, M.R., 1991. Uranium in the oceans - where it goes and why. Geochim. Cosmochim. Acta 55 (7), 1799–1806.
Kunzendorf, H., Voss, M., Brenner, W., Andrén, T., Vallius, H., 2001. Molybdenum in sediments of the central Baltic Sea as an indicator for algal blooms. Baltica 14, 123–130.
Li, D.J., Zhang, J., Wu, Y., Liang, J., Huang, D.J., 2002. Oxygen depletion off the Changjiang (Yangtze River) Estuary. Sci. Cina Ser. D Earth Sci. 32 (8), 686–694 (in Chinese with English abstract).
Li, X.X., Bianchi, T.S., Yang, Z.S., Osterman, L.E., Allison, M.A., DiMarco, S.F., Yang, G.P., 2011. Historical trends of hypoxia in Changjiang River estuary: applications of chemical biomarkers and microfossils. J. Mar. Syst. 86 (3–4), 57–68.
Liang, C., Xian, W.W., 2018. Changjiang nutrient distribution and transportation and their impacts on the estuary. Cont. Shelf Res. 165, 137–145.
Little, S.H., Vance, D., Lyons, T.W., McManus, J., 2015. Controls on trace metal authigenic enrichment in reducing sediments: Insights from modern oxygen-deficient settings. Am. J. Sci. 315 (2), 77–119.
Lu, W.H., Xiang, X.Q., Yang, L., Xu, Y., Li, X., Liu, S.M., 2017. The temporal-spatial distribution and changes of dissolved oxygen in the Changjiang Estuary and its adjacent waters for the last 50 a. Acta Oceanol. Sin. 36 (5), 90–98.
Luo, X.F., Wei, H., Fan, R.F., Liu, Z., Zhao, L.Y., Lu, Y., 2018. On influencing factors of hypoxia in waters adjacent to the Changjiang estuary. Cont. Shelf Res. 152, 1–13.
Lyons, T.W., Anbar, A.D., Severmann, S., Scott, C., Gill, B.C., 2009. Tracking euxinia in the ancient ocean: a multiproxy perspective and Proterozoic case study. Annu. Rev. Earth Planet. Sci. 37 (1), 507–534.
McManus, J., Berelson, W.M., Klinkhammer, G.P., Hammond, D.E., Holm, C., 2005. Authigenic uranium: relationship to oxygen penetration depth and organic carbon rain. Geochim. Cosmochim. Acta 69 (1), 95–108.
McManus, J., Berelson, W.M., Severmann, S., Poulson, R.L., Hammond, D.E., Klinkhammer, G.P., Holm, C., 2006. Molybdenum and uranium geochemistry in continental margin sediments: paleoproxy potential. Geochim. Cosmochim. Acta 70, 4643–4662.
Melzner, F., Thomsen, J., Koeve, W., Oschlies, A., Gutowska, M.A., Bange, H.W., Hansen, H.P., Körtzinger, A., 2013. Future ocean acidification will be amplified by hypoxia in coastal habitats. Mar. Biol. 160 (8), 1875–1888.
Morford, J.L., Emerson, S., 1999. The geochemistry of redox sensitive trace metals in sediments. Geochim. Cosmochim. Acta 63 (11 − 12), 1735–1750.
Morford, J.L., Emerson, S.R., Breckel, E.J., Kim, S.H., 2005. Diagenesis of oxyanions (V, U, Re, and Mo) in pore waters and sediments from a continental margin. Geochim. Cosmochim. Acta 69 (21), 5021–5032.
Nägler, T.F., Siebert, C., Lüschen, H., Böttcher, M.E., 2005. Sedimentary Mo isotope record across the Holocene fresh–brackish water transition of the Black Sea. Chem. Geol. 219 (1–4), 283–295.
Nameroff, T.J., Balistrieri, L.S., Murray, J.W., 2002. Suboxic trace metal geochemistry in the eastern tropical North Pacific. Geochim. Cosmochim. Acta 66 (7), 1139–1158.
Ni, X.B., Huang, D.J., Zeng, D.Y., Zhang, T., Li, H.L., Chen, J.F., 2016. The impact of wind mixing on the variation of bottom dissolved oxygen off the Changjiang Estuary during summer. J. Mar. Syst. 154, 122–130.
Noordmann, J., Weyer, S., Montoya-Pino, C., Dellwig, O., Neubert, N., Eckert, S., Paetzel, M., Böttcher, M.E., 2015. Uranium and molybdenum isotope systematics in modern euxinic basins: case studies from the central Baltic Sea and the Kyllaren fjord (Norway). Chem. Geol. 396, 182–195.
Osterman, L.E., Poore, R.Z., Swarzenski, P.W., 2008. The last 1000 years of natural and anthropogenic low-oxygen bottom-water on the Louisiana shelf, Gulf of Mexico. Mar. Micropaleontol. 66 (3–4), 291–303.
Qian, W., Dai, M.H., Xu, M., Kao, S.J., Du, C.J., Liu, J.W., Wang, H.J., Guo, L.G., Wang, L.F., 2017. Non-local drivers of the summer hypoxia in the East China Sea off the Changjiang Estuary. Estuar. Coast. Shelf Sci. 198, 393–399.
Rabalais, N.N., Diaz, R.J., Levin, L.A., Turner, R.E., Gilbert, D., Zhang, J., 2010. Dynamics and distribution of natural and human-caused hypoxia. Biogeosciences 7 (2), 585.
Rudnick, R.L., Gao, S., 2003. Composition of the continental crust. In the Crust (ed. R.L. Rudnick). In: Holland, H.D., Turekian, K.K. (Eds.), 3 Treatise on Geochemistry. Elsevier-Pergamon, Oxford, pp. 1–64.
Ross, D.A., Degens, E.T., MacIlvaine, J., 1970. . Black Sea: recent sedimentary history. Science 170 (3954), 163–165.
Sanchez-Cabeza, J.A., Ruiz-Fernández, A.C., 2012. ^{210}Pb sediment radiochronology: an integrated formulation and classification of dating models. Geochim. Cosmochim. Acta 82, 183–200.
Scott, C., Lyons, T.W., 2012. Contrasting molybdenum cycling and isotopic properties in euxinic versus non-euxinic sediments and sedimentary rocks: refining the paleoproxies. Chem. Geol. 324–325, 19–27.
Shao, L., Meng, A.H., Li, Q.Y., Qiao, P.J., Cui, Y.C., Cao, L.C., Chen, S.H., 2017. Detrital zircon ages and elemental characteristics of the Eocene sequence in IODP Hole U1435A: Implications for rifting and environmental changes before the opening of the South China Sea. Mar. Geol. 394, 39–51.
SOA (State Oceanic Administration of China), 2015. Bulletin of China Marine Environmental Status in 2000–2015. http://www.soa.gov.cn/zwgk/hygb/zghyhjzlgb/.
Sohlenius, G., Westman, P., 1998. Salinity and redox alternations in the northwestern Baltic proper during the late Holocene. Boreas 27 (2), 101–114.
Song, G.D., 2008. Climatological Parameters Distributions of Dissolved Oxygen in the East China Sea and its Application in the Oceanography. Master thesis. Ocean University of China (in Chinese with English abstract).
Stramma, L., Schmidtko, S., Levin, L.A., Johnson, G.C., 2010. Ocean oxygen minima expansions and their biological impacts. Deep Sea Res., Part I 57 (4), 587–595.
Su, C.C., Huh, C.A., 2002. ^{210}Pb, ^{137}Cs and ^{239,240}Pu in East China Sea sediments: sources, pathways and budgets of sediments and radionuclides. Mar. Geol. 183 (1–4), 163–178.
Sundby, B., Martinez, P., Gobeil, C., 2004. Comparative geochemistry of cadmium, rhenium, uranium, and molybdenum in continental margin sediments. Geochim. Cosmochim. Acta 68 (11), 2485–2493.
Swarzenski, P.W., Campbell, P.L., Osterman, L.E., Poore, R.Z., 2008. A 1000-year sediment record of recurring hypoxia off the Mississippi River: the potential role of terrestrially-derived organic matter inputs. Mar. Chem. 109 (1–2), 130–142.
Takematsu, N., Sato, Y., Okabe, S., Nakayama, E., 1985. The partition of vanadium and molybdenum between manganese oxides and sea water. Geochim. Cosmochim. Acta 49 (11), 2395–2399.
Tang, H., 2009. Studies of Eutrophication Features and Eutrophication-HABs Relationship in the Changjiang Estuary and its Adjacent Area during the Past 30 Years and Strategies on Controlling Eutrophication. Ocean University of China, Qingdao (in Chinese with English abstract).
Thomson, J., Jarvis, I., Green, D.R.H., Green, D.A., Clayton, T., 1998. Mobility and immobility of redox-sensitive elements in deep-sea turbidites during shallow burial. Geochim. Cosmochim. Acta 62 (4), 643–656.
Tribovillard, N.P., Algeo, T.J., Lyons, T., Riboulleau, A., 2006. Trace metals as paleoredox and paleoproductivity proxies: an update. Chem. Geol. 232 (1–2), 12–32.
Tyson, R.V., Pearson, T.H., 1991. Modern and ancient continental shelf anoxia: an overview. Geol. Soc. Lond. Spec. Publ. 58 (1), 1–24.
Van der Weijden, C.H., 2002. Pitfalls of normalization of marine geochemical data using a common divisor. Mar. Geol. 184 (3–4), 167–187.
Vallius, H., Kunzendorf, H., 2001. Sediment surface geochemistry of three Baltic Sea deep basins. AMBIO 30 (3), 135–142.
Wang, B.D., 2009. Hydromorphological mechanisms leading to hypoxia off the Changjiang estuary. Mar. Environ. Res. 67 (1), 53–58.
Wang, D., Sañudo Wilhelmy, S.A., 2009. Vanadium speciation and cycling in coastal waters. Mar. Chem. 117 (1–4), 52–58.
Wang, B.D., Wei, Q.S., Chen, J.F., Xie, L.P., 2012. Annual cycle of hypoxia off the Changjiang (Yangtze River) Estuary. Mar. Environ. Res. 77, 1–5.

Wang, F.F., Liu, J., Qiu, J.D., Wang, H., 2014. Historical evolution of hypoxia in East China Sea off the Changjiang (Yangtze River) estuary for the last ~13,000 years: evidence from the benthic foraminiferal community. Cont. Shelf Res. 90, 151–162.
Wang, H.J., Dai, M.H., Liu, J.W., Kao, S.J., Zhang, C., Cai, W.J., Wang, G.Z., Qian, W., Zhao, M.X., Sun, Z.Y., 2016. Eutrophication-driven hypoxia in the East China Sea off the Changjiang Estuary. Environ. Sci. Technol. 50 (5), 2255–2263.
Wang, B., Chen, J.F., Jin, H.Y., Li, H.L., Huang, D.J., Cai, W.J., 2017. Diatom bloom-derived bottom water hypoxia off the Changjiang estuary, with and without typhoon influence. Limnol. Oceanogr. 62.
Wei, H., He, Y.C., Li, Q.J., Liu, Z.Y., Wang, H.T., 2007. Summer hypoxia adjacent to the Changjiang Estuary. J. Mar. Syst. 67 (3–4), 292–303.
Wei, Q.S., Wang, B.D., Yu, Z.G., Chen, J.F., Xue, L., 2016. Mechanisms leading to the frequent occurrences of hypoxia and a preliminary analysis of the associated acidification off the Changjiang estuary in summer. Sci. Cina Earth Sci. 60 (2), 360–381.
Xu, S.M., Zhai, S.K., Zhang, A.B., Zhang, X.D., Zhang, H.J., 2007. Distribution and environment significance of redox sensitive trace elements of the Changjiang Estuary hypoxia zone and its contiguous sea area. Acta Sedimentol. Sin. 25 (5), 759–766 (in Chinese with English abstract).
Yang, S.L., Milliman, J.D., Li, P., Xu, K., 2011. 50,000 dams later: erosion of the Yangtze River and its delta. Glob. Planet. Chang. 75 (1–2), 14–20.
Yang, S.Y., Tang, M., Yim, W.W.S., Zong, Y.Q., Huang, G.Q., Switzer, A.D., Saito, Y., 2011. Burial of organic carbon in Holocene sediments of the Zhujiang (Pearl River) and Changjiang (Yangtze River) estuaries. Mar. Chem. 123 (1–4), 1–10.
Zhang, X.D., Zhai, S.K., Xu, S.M., Zhang, A.B., Lu, H.J., 2005. The “grain size effect” of redox sensitive elements in the sediments in the hypoxia zone of the Changjiang Estuary. J. Ocean Univ. China 35 (5), 868–874 (in Chinese with English abstract).
Zhang, R., Pan, S.M., Wang, Y.P., Gao, J.H., 2008. Characteristics of ^{137}Cs geochenical distribution in the subaqueous delta of the Changjiang Estuary. J. Quat. Sci. 28, 629–639.
Zhang, J., Xiao, T., Huang, D., Liu, S.M., Fang, J., 2016. Editorial: Eutrophication and hypoxia and their impacts on the ecosystem of the Changjiang Estuary and adjacent coastal environment. J. Mar. Syst. 154, 1–4.
Zhao, Y.Y., Yan, M.C., 1994. Geochemistry of Sediments of the China Shelf Sea. Science Press, Beijing.
Zhao, D.Z., Liu, J., Cheng, H.F., Wang, Z.Z., 2013. Current situation and future prospect of dredged material disposal in the Yangtze Estuary deepwater navigation channel. Hydro-Sci. Eng. 38 (2), 26–32 (in Chinese with English abstract).
Zhao, J., Feng, X.W., Shi, X.L., Bai, Y.C., Yu, X.G., Shi, X.F., Zhang, W.Y., Zhang, R.P., 2015. Sedimentary organic and inorganic records of eutrophication and hypoxia in and off the Changjiang Estuary over the last century. Mar. Pollut. Bull. 99 (1–2), 76–84.
Zhao, Y.F., Zou, X.Q., Gao, J.H., Xu, X.H., Wang, C.L., Tang, D.H., Wang, T., Wu, X.W., 2015. Quantifying the anthropogenic and climatic contributions to changes in water discharge and sediment load into the sea: a case study of the Yangtze River, China. Sci. Total Environ. 536, 803–812.
Zhao, B., Yao, P., Bianchi, T.S., Xu, Y.H., Liu, H., Mi, T.Z., Zhang, X.H., Liu, J.W., Yu, Z.G., 2017. Early diagenesis and authigenic mineral formation in mobile muds of the Changjiang Estuary and adjacent shelf. J. Mar. Syst. 172, 64–74.
Zheng, Y., Anderson, R.F., Van Geen, A., Fleisher, M.Q., 2002. Preservation of particulate non-lithogenic uranium in marine sediments. Geochim. Cosmochim. Acta 66 (17), 3085–3092.
Zhou, M.J., Shen, Z.L., Yu, R.C., 2008. Responses of a coastal phytoplankton community to increased nutrient input from the Changjiang (Yangtze) river. Cont. Shelf Res. 28 (12), 1483–1489.
Zhou, F., Huang, D.J., Ni L., X.B., Zhang, X.J., Zhu, J., K., X., 2010. Hydrographic analysis on the multi-time scale variability of hypoxia adjacent to the Changjiang River Estuary. Acta Ecol. Sin. 30 (17), 4728–4740 (in Chinese with English abstract).
Zhu, Z.Y., Zhang, J., Wu, Y., Zhang, Y.Y., Lin, J., Liu, S.M., 2011. Hypoxia off the Changjiang (Yangtze River) Estuary: Oxygen depletion and organic matter decomposition. Mar. Chem. 125 (1–4), 108–116.
Zhu, J., Zhu, Z., Lin, J., Wu, H., Zhang, J., 2016. Distribution of hypoxia and pycnocline off the Changjiang Estuary, China. J. Mar. Syst. 154, 28–40.
Zhu, Z.Y., Hu, J., Song, G.D., Wu, Y., Zhang, J., Liu, S.M., 2016. Phytoplankton-driven dark plankton respiration in the hypoxic zone off the Changjiang Estuary, revealed by in vitro incubations. J. Mar. Syst. 154, 50–56.
Zhu, Z.Y., Wu, H., Liu, S.M., Wu, Y., Huang, D.J., Zhang, J., Zhang, G.S., 2017. Hypoxia off the Changjiang (Yangtze River) Estuary and in the adjacent East China Sea: quantitative approaches to estimating the tidal impact and nutrient regeneration. Mar. Pollut. Bull. 125 (1–2), 103–114.
Zillén, L., Conley, D.J., Andrén, T., Andrén, E., Björck, S., 2008. Past occurrences of hypoxia in the Baltic Sea and the role of climate variability, environmental change and human impact. Earth-Sci. Rev. 91 (1–4), 77–92.
Zou, J.J., Shi, X.F., Li, N.S., Liu, J.H., Zhu, A.M., 2010. Early diagenetic processes of redox sensitive elements in Yangtze Estuary. Earth Sci. J. China Univ. Geosci. 35 (1), 31–42.